Defective Fast Inactivation Recovery and Deactivation Account for Sodium Channel Myotonia in the I1160V Mutant

J. E. Richmond,* D. VanDeCarr,# D. E. Featherstone,* A. L. George, Jr.,# and P. C. Ruben§
*Department of Biology, University of Utah, Salt Lake City, Utah 84112; the #Department of Pharmacology, Vanderbilt University, Nashville, Tennessee 37232; and the §Department of Biology, Utah State University, Logan, Utah 84322-5305 USA

ABSTRACT The skeletal muscle sodium channel mutant I1160V cosegregates with a disease phenotype producing myotonic discharges (observed as muscle stiffness) that are worsened by elevated K^+ levels but unaffected by cooling. The I1160V α-subunit was co-expressed with the β1-subunit in *Xenopus* oocytes. An electrophysiological characterization was undertaken to examine the underlying biophysical characteristics imposed by this mutation. Two abnormalities were found. 1) The voltage dependence of steady-state fast inactivation was reduced in I1160V, which resulted in faster rates of closed-state fast inactivation onset and recovery in I1160V compared with wild-type channels. 2) The rates of deactivation were slower in I1160V than in wild-type channels. Using a computer-simulated model, the combination of both defects elicited myotonic runs under conditions of elevated K^+, consistent with the observed phenotype of the mutant.

INTRODUCTION

There are several inherited human diseases of muscle hyperexcitability. The diseases are grouped according to clinical phenotype and exacerbating factors (Barchi, 1995; Cannon, 1996; Ptacek and Griggs, 1996). Paramyotonia congenita (PC), for example, is characterized by episodic myotonia and, less frequently, muscle weakness that occurs after muscle cooling. Hyperkalemic periodic paralysis (HyPP) is a related disorder that can involve myotonia but primarily results in periodic paralysis exacerbated by high serum potassium. Sodium channel myotonia (SCM) is a separate classification with aspects of both PC and HyPP, specifically, myotonia without muscle weakness, often exacerbated by K^+ (Lerche et al., 1993; Ptacek et al., 1994) and less frequently aggravated by cold (Heine et al., 1993). PC, HyPP, and SCM are all caused by missense mutations in voltage-gated human skeletal muscle sodium channel (hSkM1) α-subunits. Some of these mutants have been studied either in situ or in heterologous expression systems (Barchi, 1995; Cannon, 1996; Ptacek and Griggs, 1996).

In addition to the clinical importance of understanding the molecular basis of human diseases, biophysical studies of disease-causing mutant channels provide a valuable opportunity to clarify relationships between ion channel structure, biophysical performance, and in vivo function. Recent biophysical studies of muscle disease mutants have allowed new insights into the structural basis of sodium channel fast (Chahine et al., 1994; Wang et al., 1995; Ji et al., 1996) and slow inactivation (Cummins and Sigworth, 1996) as well as the physiology of muscle electrogenesis.

Like both PC and HyPP, SCM results from mutations in sodium channel regions with assigned functions. The SCM mutant V1589M, for example, is in DIV-S6, a region of the sodium channel linked to fast inactivation and drug binding (McPhee et al., 1994, 1995). Two other SCM mutations (G1306A/E) are in the DIII-IV linker crucial for fast inactivation (Lerche et al., 1993; West et al., 1992). The fast inactivation binding site is currently the object of intense interest by several groups, whose work has suggested that the binding site may consist of S4–5 linkers from several domains (Tang et al., 1996; Tang and Kallen, 1997; Lerche et al., 1997; Filatov et al., 1997; Smith et al., 1997). I1160V is an isoleucine-to-valine substitution in the domain III S4–5 linker that, like G1306A/E and V1589M, causes SCM (Ptacek et al., 1994). I1160V is of particular interest because it lies in a sodium channel region of emerging interest and importance. I1160V, however, has not been biophysically characterized.

In this study, we expressed I1160V and hSkM1 wild-type (WT) α-subunits, along with the β1-subunit, in *Xenopus* oocytes and compared the resulting currents using on-cell macropatches. On-cell macropatches of coexpressed α- and β1-subunits provide excellent voltage control and kinetic stability, resulting in fast sodium currents that closely match recordings from native channels. We examined the voltage dependence of activation and voltage dependence and rates of fast inactivation, slow inactivation, and deactivation. Our results show that, compared with hSkM1 WT, I1160V has 1) a decreased voltage sensitivity of fast inactivation at negative potentials resulting in faster recovery from inactivation and 2) slower deactivation. I1160V did not affect the voltage dependence of activation, steady-state slow inactivation, or rates of slow inactivation and did not cause a persistent current. Computer simulations of muscle membranes show that the combination of faster recovery from fast inactivation, along with slowed deactivation, is sufficient to cause potassium-sensitive myotonia, consistent with the phenotype of SCM.

Received for publication 31 March 1997 and in final form 21 July 1997.
Address reprint requests to Dr. Peter C. Ruben, Department of Biology, Utah State University, Logan, Utah 84322-5305. Tel.: 801-797-2490; Fax: 801-797-1575; E-mail: pruben@cc.usu.edu.

0006-3495/97/10/1896/08 $2.00

MATERIALS AND METHODS

cDNA for the rat brain β1-subunit was generously provided by L. Isom (Isom et al., 1992).

Mutagenesis

Site-directed mutagenesis of hSkM1 using a one-step recombinant polymerase chain reaction (PCR) strategy was performed to create the I1160V mutation. A forward primer (5′-GTG AAC GCC CTC CTA GGC GCC ATC CCC TCC GTG ATG AAT GTG CTG CTT GTC T-3′) spanning nucleotides (nts) 3525–3576 and a reverse primer (5′-TAG AGG TAC ATG TAG AG-3′, nts 3882–3898) were used to create the mutation and incorporate natural restriction sites for *Avr*II (nt 3537) and *Sse*8387I (nt 3794) in the final 373-bp product. Amplifications (20 cycles) were performed using 20 ng of hSkM1 cDNA as template and *Taq* DNA polymerase. Final products were purified by spin-column chromatography (Qiagen, Chatsworth, CA) and digested with *Avr*II and *Sse*8387I, and the resulting 257-bp fragment was ligated into the corresponding sites in the plasmid pSP64T-hSkM1. The amplified region was sequenced entirely in the final construct to verify the mutation and to exclude polymerase errors.

RNA preparation and injection

cDNAs for the WT and I1160V hSkM1 α-subunits were linearized with *Eco*R1, and β-subunit with *Hin*dIII. RNA from full-length 6.1-kb human SkM1 sodium channel α-subunit cDNA in pSP64T was synthesized in vitro with SP6 polymerase. β-Subunit cDNA in pBluescript was transcribed in vitro with T3 polymerase. In vitro transcriptions were performed on each clone. mMessage mMachine kits from Ambion (Austin, TX) were used on 1 μg of each linearized clone template. RNA for injection was precipitated and resuspended in 1 mM Tris-Cl, pH 6.5, at a concentration of approximately 1 μg/μl. Equal volumes of α- and β-subunit mRNA (each at a concentration of approximately 1 μg/μl) were mixed together before injection for both WT and mutant experiments.

Stage V-VI oocytes were surgically removed from female *Xenopus laevis* (Nasco, Modesto, CA) anesthetized with 0.17% tricaine methanesulfonate (Sigma Chemical Co., St. Louis, MO). After surgery, frogs were allowed to recover in isolation in a shallow tank of distilled water. After verifying full recovery a few hours later, frogs were returned to the large rearing tank. Theca and follicle cells were enzymatically removed from the oocytes by gently agitating the oocytes in a solution containing (in mM): 96 NaCl, 2 KCl, 20 $MgCl_2$, 5 HEPES, pH 7.4, with 2 mg/ml collagenase (Sigma) for approximately 1 h. After enzymatic treatment, oocytes were rinsed several times in a solution containing (in mM): 96 NaCl, 2 KCl, 20 $MgCl_2$, 5 HEPES, pH 7.4, and then placed in sterile incubation media containing (in mM): 96 NaCl, 2 KCl 2, 20 $MgCl_2$, 1.8 $CaCl_2$, 5 HEPES, 2.5 pyruvic acid, pH 7.4, with 1–5% horse serum (Irvine Scientific, Irvine, CA) and 100 mg/L gentamycin sulfate at 18°C. Approximately 24 h after enzymatic treatment, oocytes were individually injected with 50 nl of mRNA, using a Drummond automatic injector, and then further incubated in 60-mm disposable petri dishes with gentle agitation (approximately 60 rpm on a small rotary shaker) at 18°C until electrophysiological recording 3–14 days later. The incubation solution bathing the oocytes was changed daily.

Electrophysiology

In preparation for macropatch recording, the vitelline membrane was manually removed from oocytes after a short (2–5 min) exposure to a hyperosmotic solution containing (in mM): 96 NaCl, 2 KCl, 20 $MgCl_2$, 5 HEPES, 400 mannitol, pH 7.4. All macropatch recording was done in a chamber containing (in mM): 96 NaCl, 88 KCl, 11 EGTA, 5 HEPES, pH 7.4. Aluminosilicate patch electrodes were pulled on a Sutter P-87, dipped in melted dental wax to reduce capacitance, fire polished, and filled with (in mM): 96 NaCl, 4 KCl, 1 $MgCl_2$, 1.8 $CaCl_2$, 5 HEPES, pH 7.4.

Electrophysiological recordings were made using an EPC-9 patch-clamp amplifier (HEKA, Lambrecht, Germany) and digitized at 5 KHz (bandwidth before digitization was 1 MHz) via an ITC-16 interface (Instrutech, Great Neck, NY). Voltage clamping and data acquisition were controlled via Pulse software (HEKA) running on a Power Macintosh 7100/80. All data were software-low-pass-filtered at 5 KHz during acquisition. Experimental bath temperature was maintained at 22 ± 0.2°C for all experiments by using a peltier device controlled by an HCC-100A temperature controller (Dagan, Minneapolis, MN). After seal formation, patches were left on-cell for all recordings. On-cell patches were more stable, allowing long-term recordings, and because of equal cytosolic and extracellular [K^+], showed no differences in sodium currents or voltage dependence compared with excised inside-out patches. Where the voltage dependence of inactivation was studied, the clamp control software (Pulse) alternated prepulse potentials, such that prepulse potentials were delivered as −160 mV, +10 mV, −155 mV, +5 mV, −150 mV, etc. over the voltage range of −160 mV to +10 mV in 5 mV steps. As described in the text, prepulses were 500 ms long for steady-state fast inactivation and 1 min for steady-state slow inactivation. Holding potential was −120 mV to −150 mV. Leak subtraction was performed automatically by the software using a p/4 protocol. Leak holding potential was −120 mV. Leak pulses were always performed after the test pulse and sufficient time between protocols was allowed to insure that the leak pulses would have no effect on the data.

Analysis

Analysis and graphing were done using Pulsefit (HEKA) and Igor Pro (Wavemetrics, Lake Oswego, OR), both run on a Power Macintosh 7100/80. All statistically derived values in the text are given as mean ± standard deviation (SD) and in figures as mean ± standard error of the mean (SEM). Conductance-voltage curves were computed using the equation:

$$G = I_{max}/(V_m - E_{rev}),$$

where G is conductance, I_{max} represents the peak test pulse current, V_m the test pulse voltage, and E_{rev} the measured reversal potential.

Steady-state activation and fast inactivation were fit by a Boltzmann distribution, as follows:

$$\text{Normalized current amplitude} = 1/1 + \exp(-ze_0(V_m - V_{1/2})/kT)),$$

where normalized current amplitude is measured during a variable-voltage test pulse from a holding potential of −150 mV (for steady-state activation) or during a test pulse to 0 mV after a variable-voltage prepulse (for steady-state inactivation). V_m is the test pulse/prepulse potential, z is the apparent valence, e_0 is the elementary charge, $V_{1/2}$ is the midpoint voltage, k is the Boltzmann constant, and T is absolute temperature.

Descriptions of test pulse inactivation rates, given as time constants (τ), were derived from fitting the monoexponential decay of individual currents according to the function:

$$I(t) = I_{ss} + a_1 \exp(-t/\tau),$$

where $I(t)$ is current amplitude as a function of time, I_{ss} is the steady-state current, or asymptote (plateau amplitude), a_1 is the amplitude at time = 0 (time of peak current), and τ is the time constant (in ms).

Time constants for the onset (and recovery) of inactivation were measured in the same way, except that fits were to peak current amplitude versus prepulse (or interpulse) duration. Descriptions of first-order, two-state reaction kinetics were derived by fitting t versus voltage curves according to the following equation:

$$\tau(V_m) = 1/(k_f + k_b),$$

where $\tau(V_m)$ represents the time constant of progression to equilibrium as a function of membrane potential, k_f is the rate of the forward reaction (not

inactivated → inactivated), and k_b is the rate of the backward reaction (inactivated → not inactivated).

$$k_f = A \exp + ((e(1 - d)(V_m - V_0))/kT)$$

$$k_b = A \exp - ((ed(V_m - V_0))/kT)$$

where A = 1/2 rate at V_0, e = total reaction valence (in electronic charge), d = fractional barrier distance, V_m = membrane potential (in mV), V_0 = midpoint potential (in mV); k = Boltzmann constant, and T = absolute temperature.

Muscle membrane simulations were performed with Simulation Control Program (SCoP) 3.5 (Simulation Resources, Berrie Spring MI), using quantitative methods originally developed by Hodgkin and Huxley (1952) and subsequently adapted for mammalian skeletal muscle by Cannon et al. (1993). Briefly, the simulated membrane potential varied as a result of combined ionic sodium, potassium, and chloride (leak) currents. Sodium channel conductance was a function of m^3h gating, and potassium channel conductance was a function of n^4 gating, where m, h, and n parameters were assumed to obey first-order kinetics, as described in Hodgkin and Huxley (1952). The voltage dependence of the transitions of m, h, and n were each defined by forward and backward rate constants according to the formulations given as equations 10, 11, and 12 in Cannon et al. (1993). In these equations, we used the gating parameters and conductances given in Table 1 of Cannon et al. (1993), which they used to successfully simulate human skeletal muscle excitability. Modified sodium channel fast inactivation and deactivation in I1160V mutant muscle fibers (this paper, Fig. 5, *B* and *D*) was simulated by defining total INa = (0.5 * INa-WT) + (0.5 * INa-I1160V). Thus, 50% of simulated channels were WT, and 50% were I1160V, as occurs in the autosomal dominant disease. INa-WT used normal gating parameters obtained from rat and human skeletal muscle, as given in Cannon et al. (1993). INa-I1160V had fast inactivation recovery rates multiplied by 1.75 and deactivation rates multiplied by 0.60. These values were calculated based on the difference between WT and I1160V fast inactivation and deactivation at −70 mV. Forward and backward rates were adjusted for temperature according to a Q10 of 2.5. This Q10 was used for both WT and mutant channels.

RESULTS

Voltage dependence of activation and fast inactivation

I1160V is associated with muscle hyperexcitability, which could be due to changes in Na^+ channel availability. Channel availability can occur as a result of shifts in the voltage dependence of activation or steady-state fast inactivation as previously observed for PC and HyPP mutants (Hayward et al., 1996; Lerche et al., 1996; Yang et al., 1994; Richmond et al., 1997). Therefore, these parameters were examined in I1160V.

The conductance-voltage relationship for I1160V and hSkM1 WT is shown in Fig. 1 *A*. A test pulse potential to 0 mV was sufficient to activate approximately all channels, with the appearance of measurable currents above −70 mV. A Boltzmann distribution fit to each data set yielded the following fit coefficients (mean ± SD): I1160V, $V_{1/2}$ = −43.21 ± 6.11 mV and z = 3.44 ± 0.41; hSkM1 WT, $V_{1/2}$ = −40.4 ± 7.74 mV and z = 3.68±.0.59 (where $V_{1/2}$ is the midpoint and e is the valence of the Boltzmann distribution). These data showed no significant difference between the voltage dependence of activation in I1160V or hSkM1 WT channels using Student's t-test.

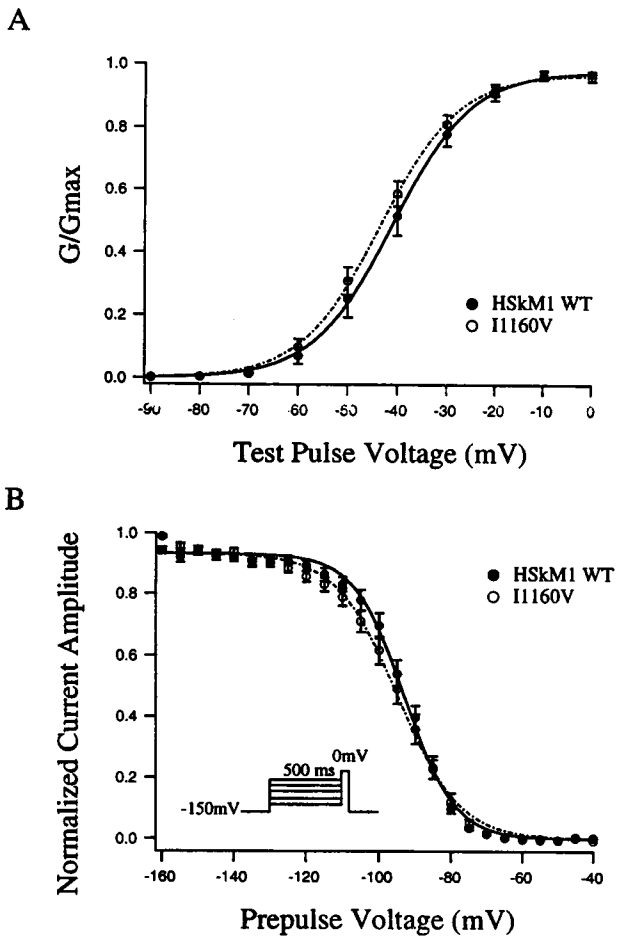

FIGURE 1 The conductance-voltage (G-V) relationship and steady-state fast-inactivation curve for I1160V and hSkM1 WT. (*A*) The voltage dependence of activation for I1160V (n = 15) and hSkM1 WT (n = 13) was measured as the fraction of channels that open in response to a 10-ms test pulse ranging between −90 and +20 mV from a V_{hold} of −150 mV (average ± SEM). (*B*) The voltage dependence of steady-state fast inactivation for I1160V (n = 21) and hSkM1 WT (n = 13) was measured as the fraction of activatable channels at 0 mV after a 500-ms prepulse ranging between −160 and −40 mV (see protocol diagram, average ± SEM).

Fig. 1 *B* shows the voltage dependence of steady-state fast inactivation for I1160V and hSkM1 WT using a prepulse duration of 500 ms (Richmond et al., 1997). Boltzmann fits yielded the following coefficients (mean ± SD): I1160V, $V_{1/2}$ = −96.6 ± 8.2 mV and z = 3.06 ± 0.46; hSkM1 WT, $V_{1/2}$ = −95.3 ± 8.3 mV and z = 3.63 ± 0.26. These data reveal a significant difference in the valence of fast inactivation (p = 0.02, Student's t-test), I1160V showing slightly lower voltage sensitivity. There was no significant difference in the midpoint of the steady-state fast inactivation curves between I1160V and hSkM1 WT.

Kinetics of fast inactivation

The myotonic discharge characteristic of PC mutants has been partially attributed to slowed open-state fast inactiva-

tion and increased rates of recovery from fast inactivation (Chahine et al., 1994; Yang et al., 1994; Hayward et al., 1996). Fast inactivation kinetics were, therefore examined in I1160V. Fig. 2 *A* shows representative series of currents evoked by test pulses between −90 and +20 mV. In most current traces a single exponential function was sufficient to fit the current decay. In some macropatches a very small residual slow mode component was also observed. The time constants of inactivation plotted in Fig. 2 *B*, derived from single exponential fits to the test pulse current decay, showed no significant difference between I1160V and hSkM1 WT.

Evidence for a persistent current was assessed by measuring the steady-state current amplitude (I_{ss}) derived from the fit expressed as a percentage of the peak current amplitude in each trace. Persistent current was negligible in both I1160V and hSkM1 WT, with average values between −40 to +20 mV of 0.2 ± 0.36% and 0.55 ± 0.12% (mean ± SD), respectively. There was no significant difference between persistent current values obtained for hSkM1 WT and I1160V at any of these voltages.

To examine the kinetics of closed-state fast inactivation, prepulses of varying duration between −100 mV and −60 mV were used, before a test pulse at 0 mV as exemplified in the right panel of Fig. 2 *C* for a prepulse of −80 mV. Recovery from fast inactivation (exemplified in the left panel of Fig. 2 *C*) was examined by fast inactivating all channels with a 500-ms pulse to 0 mV before a prepulse of

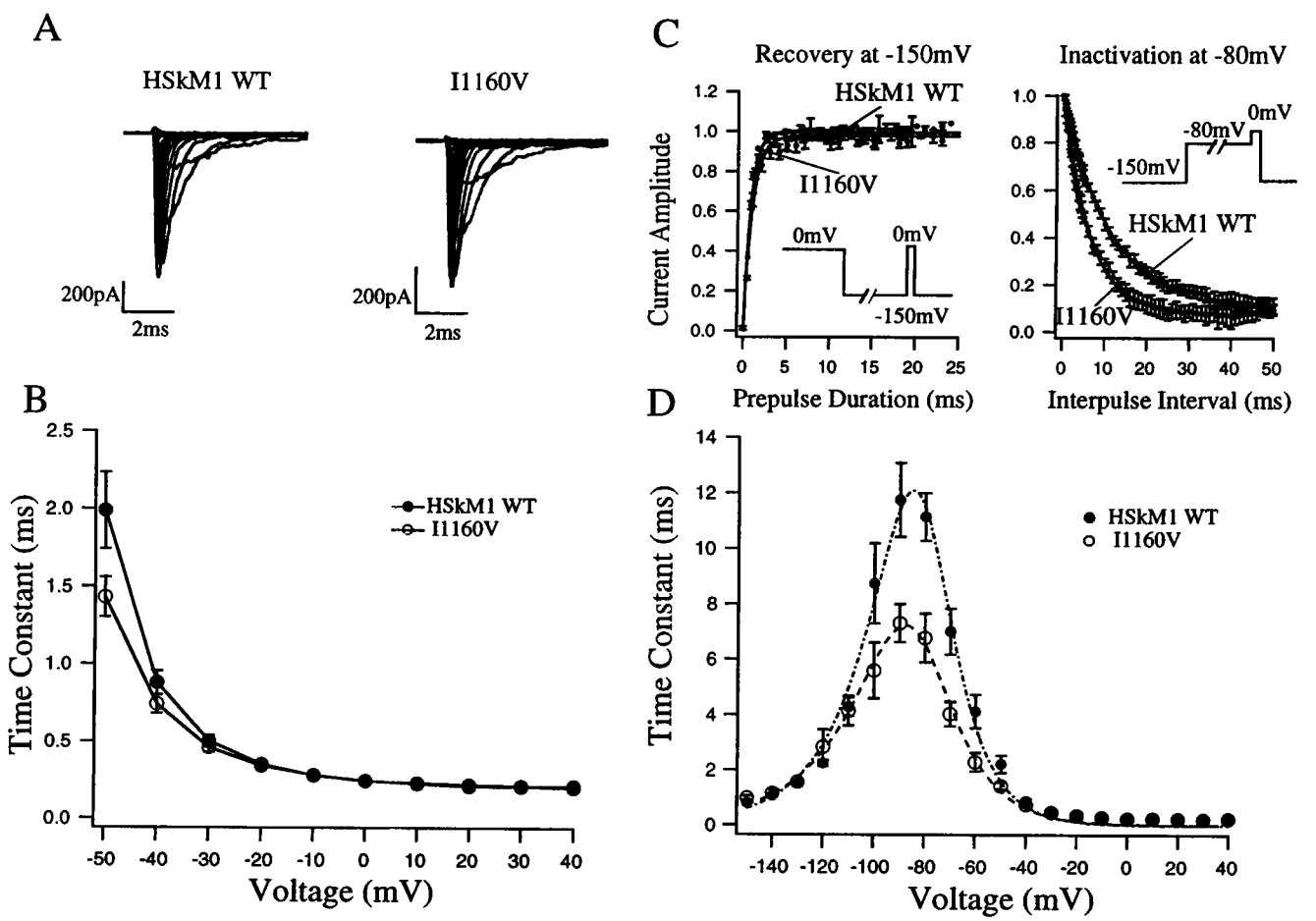

FIGURE 2 Inactivation kinetics of I1160V and hSkM1 WT sodium channels. (*A*) Representative macropatch sodium currents evoked by test pulses from −150 mV to a series of potentials ranging from −90 mV to +20 mV for hSkM1-WT and I1160V sodium channels. (*B*) Single exponentials were fit to test pulse decay at voltages from −50 mV to +40 mV to derive the time constants for open-state fast inactivation (average ± SEM; *n* for I1160V ranging from 15 to 22 and hSkM1 WT ranging from 5 to 10 for voltages −50 mV to +40 mV). (*C, left panel*) Normalized currents for fast-inactivation recovery at −150 mV in I1160V ($n = 9$) and hSkM1 WT ($n = 10$) channels (average ± SEM). Current values were obtained from 0-mV test pulses after a −150-mV interpulse of varying duration, where the interpulse followed a 500-ms step to 0 mV, which fully inactivated all channels (see protocol diagram). (*C, right panel*) Averaged, normalized currents for the onset of closed-state fast inactivation at −80 mV for I1160V ($n = 5$) and hSkM1 WT ($n = 7$; average ± SEM). Normalized current amplitudes were derived from 0-mV test pulses after a −80 mV prepulse of increasing duration (see protocol diagram). Fit lines were derived by fitting a single exponential to the normalized, averaged plots of 0-mV test pulse amplitude versus prepulse duration. (*D*) The time constants of closed-state fast inactivation (*n* for I1160V ranging from 4 to 5 and for hSkM1 WT ranging from 5 to 9 for voltages from −100 mV to −60 mV) and test pulse fast inactivation (−50 mV through +60 mV, *n* given in *B*) and recovery (*n* for I1160V ranging from 3 to 9 and for hSkM1 WT ranging from 5 to 10 for voltages from −150 mV to −110 mV). I1160V (○) and hSkM1 WT (●) are plotted as a function of voltage (average ± SEM). Time constants for closed-state fast inactivation and recovery were derived from exponential fits to 0-mV test pulses versus duration for each voltage on individual macropatches. Fit lines to the ensemble time constant data are predictions of a first-order Eyring reaction model.

varying duration to a recovery potential within the range −150 to −110 mV, followed by a test pulse to 0 mV to assay the fraction of recovered channels. Averaged time constants derived from single exponential fits to data as in Fig. 2 *C* are plotted in Fig. 2 *D* over the entire voltage range tested (−150 to −60 mV), along with the open-state fast inactivation τ values (between −50 mV and +40 mV). A two-state (not inactivated to inactivated) first-order Eyring reaction model was used to fit the averaged time constant data for I1160V and hSkM1 WT. The coefficients of this fit gave a maximal time constant of 7.04 ms for I1160V vs. 11.8 ms for hSkM1 WT, showing that the fast inactivation time constants around the peak of the reaction are faster in I1160V.

At potentials negative to −100 mV, the rates of inactivation in I1160V were not significantly different from hSkM1 WT. Statistical analysis (*t*-test) of the time constants (mean ± SD) of the inactivation bell-shaped curve between −90 mV and −70 mV confirmed that the average values over this range were significantly different for I1160V compared with wild-type channels.

As previously demonstrated (Featherstone et al., 1996), the rates of inactivation derived from the fast inactivation onset and recovery protocols at the same voltages overlap, as these rates reflect the progress of the inactivation reaction toward equilibrium. Therefore, time constants graphed in the bell-shaped curve reflect either fast inactivation or recovery depending on the initial state of the channel, i.e., either initially inactivated in the recovery protocol or initially not inactivated in the onset protocol. After the peak of an action potential, time constants would largely reflect recovery from inactivation.

Deactivation kinetics

It has been shown that deactivation rates are also affected in several PC mutants (Hayward et al., 1996; Ji et al., 1996; Featherstone et al., submitted). In the PC mutants R1440P and R1440C, which have identical fast inactivation rates, the degree of slowing of deactivation corresponds to the severity of the disease phenotype (Featherstone et al., submitted). Furthermore, inclusion of slowed deactivation rates in a muscle simulation demonstrated that deactivation is an important contributor to the temperature sensitivity of muscle hyperexcitability in these PC mutants (Featherstone et al., submitted).

To measure the deactivation rates in I1160V and hSkM1 WT, channels were initially opened with a brief step (0.5 ms) to +50 mV before command potentials ranging from −120 to −30 mV, which produced tail currents (see protocol diagram in Fig. 3 *A*). Fig. 3 *A* shows representative examples of tail currents at −80 mV for I1160V and hSkM1 WT. At all potentials tested, the tail current decay in I1160V (mean ± SD) was significantly slower than hSkM1 WT using Student's *t*-test (Fig. 3 *B*).

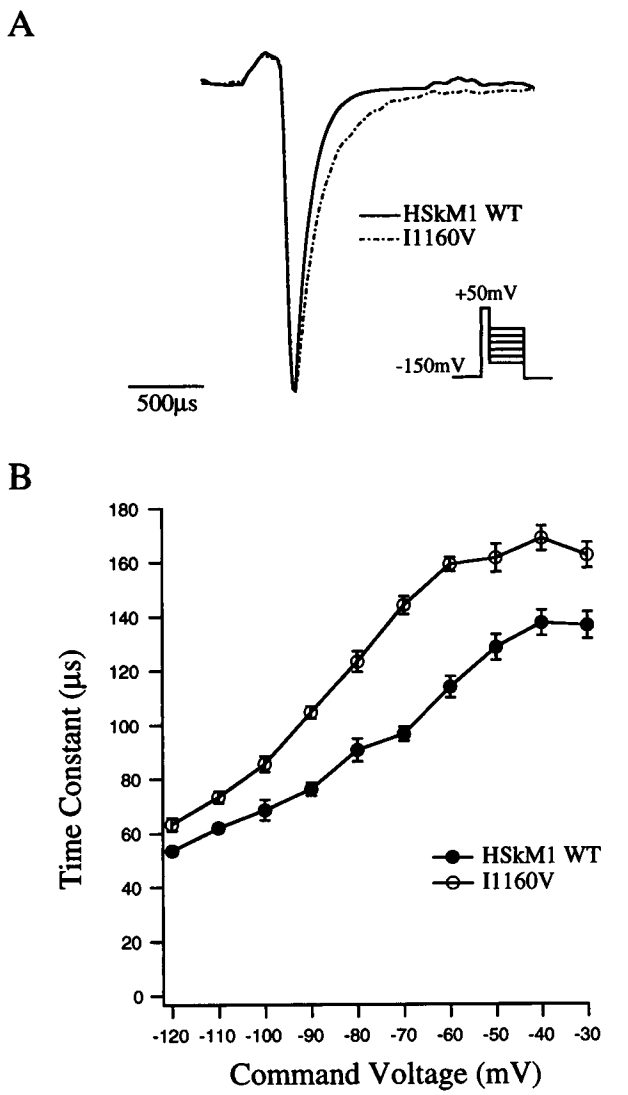

FIGURE 3 Deactivation rates of I1160V and hSkM1 WT. (*A*) Typical tail currents during a step to −60 mV, after a brief (0.5-ms) channel-opening pulse to +50 mV for I1160V and hSkM1 WT (see protocol diagram in figure). (*B*) Single exponentials were fit to tail current decays to derive the average ± SEM time constants of deactivation for I1160V (n = 12) and hSkM1 WT (n = 8) over the voltage range shown.

Fast inactivation has been shown to contribute to tail current decay (Aldrich and Stevens, 1987). However, using the IFM to QQQ mutation of the skeletal muscle sodium channel we know that contributions to tail currents would only occur at potentials more positive than −80 mV (Featherstone et al., submitted). At voltages more negative than −80 mV, the extremely significant differences in deactivation rates in I1160V compared with hSkM1 WT are unequivocally due to differences in deactivation rates. At more positive potentials, open-state fast inactivation rates for I1160V and hSkM1 WT are identical (see Fig. 2 *B*). Therefore, the differences in decay rates over this range, regardless of any contribution due to fast inactivation decay, can also be attributed to a significant slowing of deactivation in I1160V.

Steady-state slow inactivation

In the HyPP mutant T704M, it has been shown that the rates and extent of slow inactivation are affected (Cummins and Sigworth, 1996; Hayward et al., 1997). Less complete slow inactivation in combination with a small persistent current in T704M has been speculated to account for the prolonged muscle depolarization and resultant muscle paralysis characteristic of the HyPP phenotype (Cummins and Sigworth, 1996). In the PC mutant T1313M, in which muscle paralysis is less common, persistent currents have been observed in some studies (Tahmoush et al., 1994; Hayward et al., 1996) although not in others (Richmond et al., 1997; Yang et al., 1994), but steady-state slow inactivation is not affected. As 20% of both hSkM1 WT and PC mutant channels do not slow inactivate at steady state (Richmond et al., 1997), a persistent current could still bring about some degree of muscle paralysis. I1160V is not associated with muscle weakness, and in our study there is also no evidence of a persistent current. However, it is possible that slow inactivation could still be affected in I1160V without any apparent phenotypic consequence. Due to the similar location of I1160V in DIII with respect to T704M in DII (Cannon, 1996), it was important to examine slow inactivation in I1160V.

To measure steady-state slow inactivation, a prepulse of 60 s was followed by a 5-ms step to −150 mV (to recover channels from fast inactivation) before a 0-mV test pulse to assay for slow inactivation. A 30-s step back to −150 mV was included between trials to fully recover channels from slow inactivation (Featherstone et al., 1996). As shown in Fig. 4 *A*, steady-state slow inactivation in I1160V assessed with Student's *t*-test was not significantly different from hSkM1 WT.

Slow inactivation kinetics

Rates of slow inactivation were measured at prepulse voltages ranging from −90 to 0 mV. A prepulse of increasing duration (0–60 s) was used to induce inactivation followed by a 5-ms step to −150 mV (to recover fast-inactivated channels) before a test pulse to assay for the fraction of available channels. A 30-s step back to −150 mV was used between trials to fully recover all channels from slow inactivation. At all potentials, slow inactivation was complete by 60 s. A single exponential fit to these plots yielded the time constants of slow inactivation for each prepulse voltage from −90 to 0 mV graphed in Fig. 4 *B*.

The time constants of recovery from slow inactivation were measured at prepulses between −150 and −110 mV. A 60-s conditioning pulse to 0 mV was used to maximally slow inactivate all channels, followed by a prepulse of varying duration; a 5-ms step to −150 mV selectively recovered all fast-inactivated channels, so that a final test pulse assayed for the fraction of slow-inactivated channels only. A 30-s step back to −150 mV between trials was used to recover all channels from slow inactivation. Plots of prepulse duration versus test pulse current amplitude were fit with a single exponential to determine the time constants

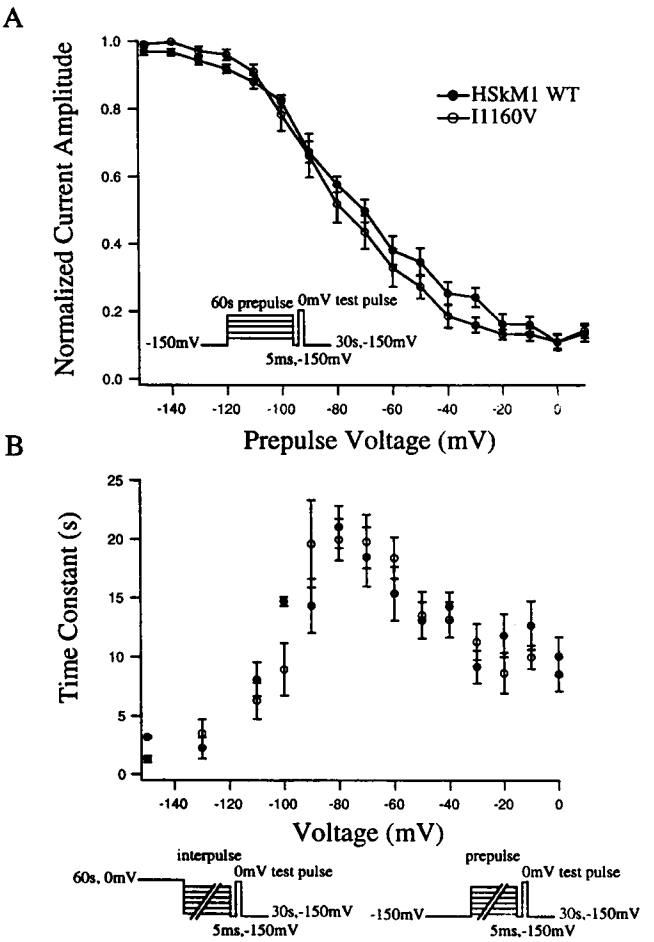

FIGURE 4 Slow inactivation kinetics and steady-state voltage dependence of I1160V and hSkM1 WT. (*A*) Steady-state slow inactivation plotted as a function of voltage for I1160V (n = 9) and hSkM1 WT (n = 23; average and SEM). At each voltage, a prepulse of 60 s was followed by a 5-ms step to −150 mV to selectively recover fast inactivation before a test pulse to assay for slow inactivation and a 30-s step back to −150 mV to recover from all inactivation (see protocol diagram in *A*). (*B*) Time constants of slow inactivation plotted as a function of voltage for I1160V and hSkM1 WT. The onset of slow inactivation was measured at prepulse voltages ranging from −90 to 0 mV (n for I1160V ranging from 4 to 11 and for hSkM1 WT ranging from 4 to 12). A prepulse of varying duration (0 to 60 s) was used to induce inactivation followed by a 5-ms step to −150 mV (to recover fast-inactivated channels) before a test pulse to assay for available channels. A 30-s step back to −150 mV was used to recover from slow inactivation (see right protocol diagram in *B*). The time constants of recovery from slow inactivation were measured at prepulses between −150 and −110 mV (n for I1160V ranging from 3 to 5 and for hSkM1 WT ranging from 3 to 8). A 60-s conditioning pulse to 0 mV was used to maximally slow-inactivate all channels, followed by a prepulse of varying duration; a 5-ms step to −150 mV selectively recovered all fast-inactivated channels, so that a final test pulse assayed for slow inactivated channels only. A 30 s step back to −150 mV was used to recover from residual slow inactivation (see left protocol diagram in *B*). Slow inactivation onset and recovery time constants were measured by fitting single exponentials to plots of peak test pulse current amplitude versus prepulse duration. In each case, slow inactivation was best fit by a single exponential.

of slow-inactivation recovery plotted over the range −150 to −110 mV in Fig. 4 *B*.

The kinetics of slow inactivation were not significantly different between I1160V and hSkM1 WT with the exception of time constants at −150 mV.

Computer simulations of biophysical parameters observed in I1160V and hSkM1 WT

To test the effects of the I1160V inactivation and deactivation defects, voltage recordings from an excitable muscle membrane were computer simulated (Fig. 5). For these simulations, standard Hodgkin-Huxley equations were used, except that rates, concentrations, conductances, and Q10 values from rat and human skeletal muscle were incorporated (see Table 1 of Cannon et al., 1993; Hayward et al., 1996). The rate of recovery from fast inactivation for I1160V was increased to 1.75 of the hSkM1 WT rate, and the deactivation rate was decreased to 0.6 that of hSkM1 WT based on the presented biophysical observations using the time constants at −70 mV (see Figs. 2 and 3).

At normal K^+ levels (4 mM) a 20-ms, 160 uA/cm^2 stimulus elicited a single action potential in both the hSkM1 WT and I1160V simulations (Fig. 5, *A* and *B*, respectively). When external K^+ was elevated to 12 mM, the I1160V mutant produced an action potential barrage (Fig. 5 *D*), whereas hSkM1 WT was unaffected (Fig. 5 *C*). The myotonia was observed only when both deactivation and fast-inactivation recovery were altered to reflect the observations in Figs. 2 and 3. Either defect alone was insufficient to produce myotonia in the simulation.

In similar simulations of PC mutants R1440C and R1440P, which exhibit cold-induced myotonia, defects in deactivation and open-state fast inactivation produced myotonic runs at lowered temperatures (from 37°C to 27°C; see Featherstone et al., submitted). Reducing the temperature to 27°C in the I1160V simulation did not produce muscle hyperexcitability at normal K^+ levels, consistent with the lack of temperature sensitivity of the I1160V phenotype.

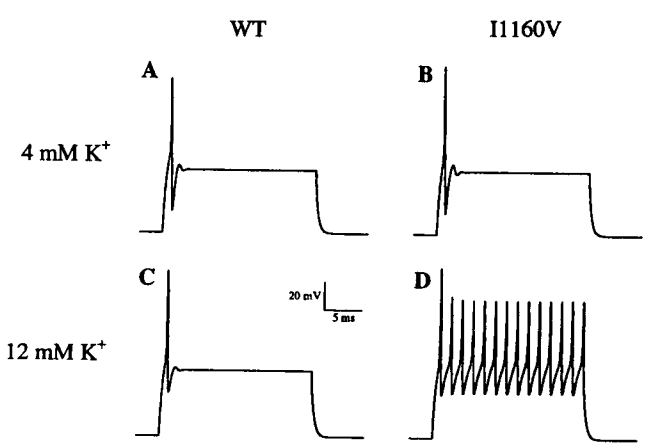

FIGURE 5 A computer simulation incorporating the biophysical defects observed in I1160V compared with hSkM1 WT. The rate of recovery from fast inactivation for I1160V was increased to 1.75 of the hSkM1 WT rate, and the deactivation rate was decreased to 0.6 that of hSkM1 WT based on the presented biophysical observations (see Figs. 2 and 3). A simulated membrane response to a 20-ms, 160 μA/cm^2 stimulus at 37°C elicited a single action potential in both hSkM1-WT (*A*) and I1160V (*B*) at physiological external K^+ levels (4 mM) and at elevated K^+ (12 mM).

DISCUSSION

The hSkM1 sodium channel mutant I1160V is associated with SCM, a disease in which K^+-aggravated myotonia occurs in the absence of muscle weakness (Ptacek et al., 1994). To gain insights into the underlying biophysical disruptions that account for SCM, the I1160V mutant was constructed and examined electrophysiologically.

We have shown that the I1160V mutation slows deactivation and lowers voltage sensitivity of fast inactivation compared with WT. Within physiologically relevant voltage ranges (approximately −90 mV to +40 mV), the lowered voltage dependence would speed recovery from fast inactivation after an action potential. This, in combination with slowed deactivation, results in K^+-sensitive, but not cold-sensitive, myotonia in computer simulations of a muscle membrane. In the model, we presumed no effect of potassium on sodium channel gating.

In addition to I1160V, three other hSkM1 mutants (G1306A, G1306E, and V1589M) have been linked to the SCM phenotype (Heine et al., 1993; Lerche et al., 1993; Ptacek and Griggs, 1996). Variations in temperature sensitivity (Heine et al., 1993) and incomplete assessment of K^+ sensitivity among the SCM mutants (Ptacek and Griggs, 1996) complicate any interpretation of common biophysical observations that may account for the SCM phenotype. In addition, the biophysical data for each of the four mutants is presently incomplete. However, three of the four mutants have been shown to have slowed deactivation (I1160V, G1306A, and G1306E; Mitrovic et al., 1995). Deactivation in the fourth mutant, V1589M, has not yet been assessed. Additionally, recovery from fast inactivation is faster in all four mutants (Mitrovic et al., 1994, 1995), although in G1306A/E, the predominant effect was at unphysiologically negative potentials (Mitrovic et al., 1995). It is tempting to speculate that the myotonia common to all four mutants is dependent on the occurrence of both slowed deactivation and faster rates of recovery from inactivation. However, several of the SCM mutants have additional defects that would also predict hyperexcitability. For example, G1306A and G1306E show slowed rates of open-state fast inactivation (Mitrovic et al., 1995). Furthermore, V1589M and G1306E have evidence of increased late openings, seen as persistent current (Mitrovic et al., 1994, 1995). Both of these parameters could augment excitability and perhaps explain differences in the degree of myotonia among mutants and the additional temperature sensitivity of V1589M.

A common finding in all four SCM mutants is the absence of muscle weakness (Ptacek and Griggs, 1996). In

HyPP, muscle weakness is attributed to a defect in slow inactivation in conjunction with a persistent current (Cummins and Sigworth, 1996). Consistent with this interpretation, I1160V has neither persistent current nor slow inactivation defects, which accounts for the lack of muscle weakness. Both G1306E and V1589M have been reported to have persistent currents, but slow inactivation has not been investigated. If a slow inactivation defect is a necessary prerequisite of mutants exhibiting muscle weakness, then a prediction would be that none of the SCM mutants would have slow inactivation defects.

The subtle biophysical changes resulting from the I1160V mutation appear to be able to account for the disease phenotype. However, the importance of the isoleucine at position 1160 to normal sodium channel function remains unclear. We can speculate, based on our results, that the slower deactivation rates in the I1160V mutation might reflect slower inward S4 translocations, which would increase the likelihood that the binding site would be available for closed-state fast inactivation to occur, thus reducing the apparent valence of fast inactivation.

We thank Esther Fujimoto for RNA preparation.
This work was supported by PHS grants NS29204 to P.C. Ruben and NS32387 to A.L. George.

REFERENCES

Aldrich, R. W., and C. F. Stevens. 1987. Voltage-dependent gating of single sodium channels from mammalian neuroblastoma cells. *J. Neurosci.* 7:418–431.

Barchi, R. L. 1995. Molecular pathology of the skeletal muscle sodium channel. *Annu. Rev. Physiol.* 57:355–385.

Cannon, S. C. 1996. Ion-channel defects and aberrant excitability in myotonia and periodic paralysis. *Trends Neurosci.* 19:3–10.

Cannon, S. C., R. H. Brown, Jr., and D. P. Corey. 1993. Theoretical reconstruction of myotonia and paralysis caused by incomplete inactivation of sodium channels. *Biophys. J.* 65:270–288.

Chahine, M., A. L. George, Jr., M. Zhou, S. Ji, W. Sun, R. L. Barchi, and R. Horn. 1994. Sodium channel mutations in paramyotonia congenita uncouple inactivation from activation. *Neuron.* 12:281–294.

Cummins, T. R., and F. J. Sigworth. 1996. Impaired slow inactivation in mutant sodium channels. *Biophys. J.* 71:227–236.

Featherstone, D. E., J. E. Richmond, and P. C. Ruben. 1996. Interaction between fast and slow inactivation in Skm1 sodium channels. *Biophys. J.* 71:3098–3109.

Filatov, G. N., S. D. Kraner, and R. L. Barchi. 1997. Secondary structure of the D4/S4–5 linker probed by systematic cysteine accessibility method. *Biophys. J.* 72:A260.

Hayward, L. J., R. H. Brown, Jr., and S. C. Cannon. 1997. Deficient slow inactivation in a subset of mutant sodium channels associated with periodic paralysis. *Biophys. J.* 72:A116.

Hayward, L. L., R. H. Brown, Jr., and S. C. Cannon. 1996. Inactivation defects caused by myotonia-associated mutations in the sodium channel III-IV linker. *J. Gen. Physiol.* 107:559–576.

Heine, R., U. Pika, and F. Lehmann-Horn. 1993. A novel SCN4A mutation causing myotonia aggravated by cold and potassium. *Hum. Mol. Genet.* 2:1349–1353.

Isom, L., L. K. S. De Jongh, D. E. Patton, B. F. X. Reber, J. Offord, H. Charbonneau, K. Walsh, A. L. Goldin, and W. A. Catterall. 1992. Primary structure and functional expression of the β1 subunit of the rat brain sodium channel. *Science.* 256:839–842.

Ji, S., A. L. George, Jr., R. Horn, and R. L. Barchi. 1996. Paramyotonia congenita mutations reveal different roles for segments S3 and S4 of domain D4 in hSkM1 sodium channel gating. *J. Gen. Physiol.* 107: 183–194.

Lerche, H., R. Heine, U. Pika, A. L. George, Jr., N. Mitrovic, M. Browatzki, T. Weis, M. Rivet-Bastide, C. Franke, M. Lomonaco, K. Rickes, and F. Lehmann-Horn. 1993. Human sodium channel myotonia: slowed channel inactivation due to substitutions for a glycine within the III-IV linker. *J. Physiol.* 470:13–22.

Lerche, H., N. Mitrovic, V. Dubowitz, and F. Lehmann-Horn. 1996. Paramyotonia congenita: the R1448P Na^+ channel mutation in adult human skeletal muscle. *Ann. Neurol.* 39:599–608.

Lerche, H., W. Peter, N. Mitrovic, R. Fleischhauer, U. Pika-Hartlaub, M. Schiebe, and F. Lehmann-Horn. 1997. Role in fast inactivation of the IV/S4–S5 loop of the human muscle sodium channel probed by cysteine mutagenesis. *Biophys. J.* 72:A260.

McPhee, J. C., D. S. Ragsdale, T. Scheuer, and W. A. Catterall. 1994. A mutation in the segment IVS6 disrupts fast inactivation of sodium channels. *Proc. Natl. Acad. Sci. USA.* 91:12346–12350.

McPhee, J. C., D. S. Ragsdale, T. Scheuer, and W. A. Catterall. 1995. A critical role for transmembrane segment IVS6 of the sodium channel α subunit in fast inactivation. *J. Biol. Chem.* 270:12025–12034.

Mitrovic, N., A. L. George, Jr., R. Heine, S. Wagner, U. Pika, U. Hartlaub, M. Zhou, H. Lerche, C. Fahlke, and F. Lehmann-Horn. 1994. K^+-aggravated myotonia: destabilization of the inactivated state of the human muscle Na^+ channel by the V1589M mutation. *J. Physiol.* 478.3:395–402.

Mitrovic, N., A. L. George, Jr., H. Lerche, S. Wagner, C. Fahlke, and F. Lehmann-Horn. 1995. Different effects on gating of three myotonia-causing mutations in the inactivation gate of the human muscle sodium channel. *J. Physiol.* 487.1:107–114.

Ptacek, L., and R. C. Griggs. 1996. Familial periodic paralysis. *In* Molecular Biology Membrane Transport Disorders. S. G. Schultz, editor. Plenum Press, New York. 625–642.

Ptacek, L. J., R. Tawil, R. C. Griggs, G. Meola, P. McManis, R. J. Barohn, J. R. Mendell, C. Harris, R. Spitzer, F. Santiago, and M. F. Leppert. 1994. Sodium channel mutations in acetazolamide-responsive myotonia congenita, paramyotonia congenita, and hyperkalemic periodic paralysis. *Neurology.* 44:1500–1503.

Richmond, J. E., D. E. Featherstone, and P. C. Ruben. 1997. Human Na^+ channel fast and slow inactivation in paramyotonia congenita mutants expressed in *Xenopus laevis* oocytes. *J. Physiol.* 499:589–600.

Smith, M. R., E. J. Yu, and A. L. Goldin. 1997. Interaction between the putative sodium channel inactivation particle and domain III S4–S5. *Biophys. J.* 72:A261.

Tahmoush, A. J., K. L. Schaller, P. Zhang, T. Hyslop, T. Heiman-Patterson, and J. H. Caldwell. 1994. Muscle sodium channel inactivation defect in paramyotonia congenita with the thr1313met mutation. *Neuromusc. Dis.* 4(5/6):447–454.

Tang, L., and R. G. Kallen. 1997. Mutations in cytoplasmic portions of sodium channels affecting inactivation: S4–5 segments. *Biophys. J.* 72:A260.

Tang, L., R. G. Kallen, and R. Horn. 1996. Role of an S4–S5 linker in sodium channel inactivation probed by mutagenesis and peptide blocker. *J. Gen. Physiol.* 108:89–104.

Wang, J., V. Dubowitz, F. Lehmann-Horn, K. Ricker, L. Ptacek, and E. P. Hoffman. 1995. In vivo channel structure/function studies: consecutive Arg1448 changes to Cys, His, and Pro at the extracellular surface of IVS4. *In* Ion Channels and Genetic Diseases. Rockefeller University Press, New York. 77–88.

West, J. W., D. E. Patton, T. Scheuer, Y. Wang, A. L. Goldin, and W. A. Catterall. 1992. A cluster of hydrophobic amino acid residues required for fast Na^+-channel inactivation. *Proc. Natl. Acad. Sci. USA.* 89: 10910–10914.

Yang, N., S. Ji, M. Zhou, L. J. Ptacek, R. L. Barchi, R. Horn, and A. L. George, Jr. 1994. Sodium channel mutations in paramyotonia congenita exhibit similar biophysical phenotypes in vitro. *Proc. Natl. Acad. Sci. USA.* 91:12785–12789.